e-ISSN: 2582-5208
International Research Journal of Modernization in Engineering Technology and Science
(Peer-Reviewed, Open Access, Fully Refereed International Journal)
Volume:06/Issue:04/April-2024 Impact Factor- 7.868 www.irjmets.com

SIMULATION OF THREE PORT DC-DC CONVERTER WITH SOLAR PV SYSTEM FED BLDC MOTOR

E. Vishnuvarthini*1, K. Logavani*2

*1PG Scholar, Power Electronics And Drives, Government College Of Engineering Salem, Tamil Nadu, India.

*2Associate Professor Department Of EEE, Government College Of Engineering, Salem, Tamil Nadu, India.

DOI : https://www.doi.org/10.56726/IRJMETS51794

ABSTRACT

The expanded requirement for renewable sources of energy systems in order to generate the power, store energy, and connect the energy storage devices with applications has turned into a major challenge. Energy storage using batteries is in the majority of suitable cases for energy sources like solar, wind, etc. In this paper, three-port converter is designed and simulated for battery energy storage, interfaced with an output drive. Based on the requirements, the power that is extracted from the solar panel during the daytime is utilized to charge the batteries through the three-port converter. The proposed three-port converter in terms of operating principles and power flow can significantly enhance the system efficiency. To develop the suggested approach's control hardware, and prototype model results are obtained to test the proposed three-port converter control system's efficiency and practicality. Overall, the efficiency of the converter's output has shown an improvement. The success rate is 96.5% when charging an ESS, 98.1% when discharging an ESS, and 95.7% overall.

Keyword: BLDC Motor; DC–DC Converter, MPP Tracking; Solar Pvsystem, Three-Portconverter (TPC), Energy Storage Device (ESD).

I. INTRODUCTION

Renewable energy is environmentally friendly, but its constant yet variable DC voltage has a disadvantage. For example, solar panels depend on the position of the sun in the sky, as well as the hours of the day, which affects not only the amount of power that is produced but also the current that is transmitted. Since the wind speed is not controllable, the output voltage of the generator is not sufficient to power the inverter directly. Therefore, the AC voltage converter (or other load) must be connected to a battery to power the output drive.

A non-isolate three port converter can be built with shared switches. The regenerative energy system is connected to a three port circuit. During the day, the solar panels collect energy and send it to the three port converter. The three port bidirectional one storage inductor charges the batteries. Multiple port converters have been studied for electric vehicles (EVs), energy storage (ES) and PV (PV). Multi-port converters need only a few conversion stages. The power density and conversion efficiency of these converters are very high when compared with conventional converters. For applications of higher power, isolated TPCs are needed. Non-isolated TPC may offer high efficiency, high power output and low cost in low power applications due to the reduction of transistors in a TPC. Single-switch TPC is a TPC family consisting of dual input/output converters with an additional power flow path. It has a very small size and high integration ratio. The two inductor bidirectional converters and two inductive boost converters combine to form a single TPC family. This TPC allows for the regulation of switching frequency as well as duty cycle. The usefulness and efficiency of the TPC are severely limited by the lack of a separate control approach, A multi-port step-up / step-down converter can be constructed with shared switches and connected to a three-port energy storage system. Different types of multi-port converter have been studied for electric vehicles (EVs), power storage (ES) and DC-to-DC converter circuits. Non-isolation TPCs offer high efficiency, high power output, and low cost in low power applications by decreasing the number of integrated transistors in a circuit. This is due to the high power density and high conversion efficiency of non-isolation bidirectional converters, which do not have isolation, but are inexpensive, easy to construct, and have limited internal components.

This TPC can be further improved and optimized with the help of the proposed magnetic integration technique. High voltage gain non-isolation TPCs are very challenging and complex in design. An important addition to this

e-ISSN: 2582-5208
International Research Journal of Modernization in Engineering Technology and Science
(Peer-Reviewed, Open Access, Fully Refereed International Journal)
Volume:06/Issue:04/April-2024 Impact Factor- 7.868 www.irjmets.com

study is the single stage power conversion that takes place between load port and PV or between load port and battery depending on the design. Power density can be improved by sharing passive power devices in different power flow modes. Efficiency can be improved by reducing the conversion gain by series connecting the PV in series with the battery during the discharge domain and making parallel connection between them during the charging domain. Generally, a PV panel is capable of producing the DC, except for most common household appliances such as fans. It can also use single phase induction motors, so conversion loss may have occurred in the operation of the DC to AC converter. This type of difficulty cannot be eliminated by replacing an AC induction motor by a DC motor.

The disadvantage of a DC motor, however, is its high maintenance cost, low rpm application and high EM (electromagnetic (noise). A BLDC is used as an alternative because it has an improved power to weight ratio over a conservative induction motor. The advantage of a BLDC is that it is openly able to power run of DC, but for speed control of a BLDC drive, it has the advantage of additional current sensors and control.

II. PROPOSED SYSTEM

2.1 CIRCUIT OF PROPOSED SYSTEM

The DC/DC Converter, In 3 Port Converter Multi-port converters are commonly used in standalone renewable power systems in order to provide continuous and stable power to the electricity loads. Full Bridge Three Port Converter (FB-TPC) Interfaces Renewable Energy Source, Storage Battery and Load.

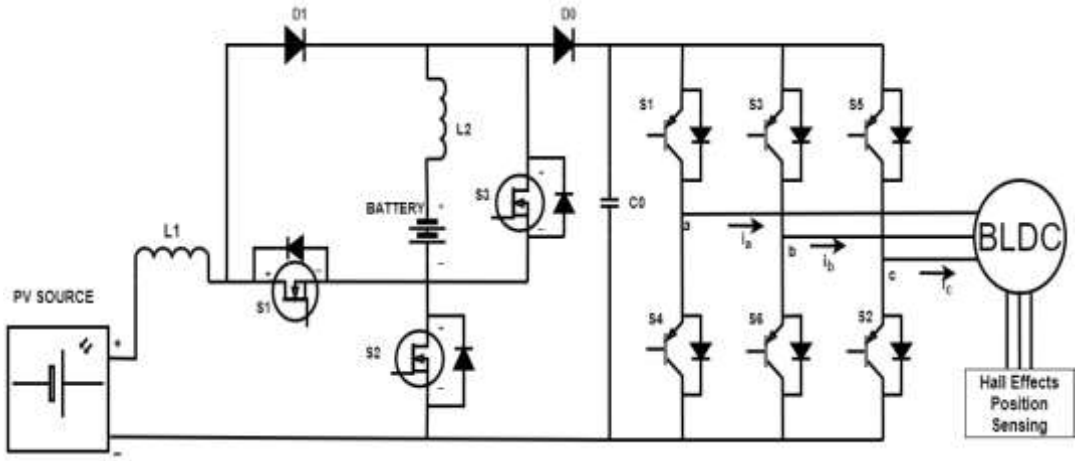

Figure 2.1: Circuit Diagram Of Proposed System

In this figure 2.1 shown the diagram of proposed system that can using the photovoltaic source act as a input and its gives to converter then universal bridge given to motor load as BLDC.

2.2 DESIGN OF CONVERTER AND OPERATING PRINCIPLES

The foundation of the converter is established by the voltage extension cell and switching circuit built around an inductor, as illustrated in Figure 2.1. The proposed converter operates in three distinct modes for each input:

- Independent power transfer between input and output;
- Simultaneous power transfer from input to output;
- Energy transmission from a power generator to a load, which is also utilized for ESS charging.

The operation of the proposed converter is determined by the ESS charging and discharging state. During discharging, the switch S2 body diode SD2 remains "OFF". Energy is transferred independently from one phase to the next. The main switches in the converter are S1 and S2, while diodes D1 and D0 conduct. The filter capacitor and inductive elements are denoted by C0, L1, and L2. In mode charging , the switch S3 and body diode SD3 is always “OFF”. The PV phases transfer energy from the inputs to the output and batteries. The primary switches in the converter are S1 and S3. Diodes D1 and D0 conduct, and the filter capacitor and inductive elements are represented by C0, L1, and L2.

To achieve the desired ripple effects, the values of inductance L1, L2, and capacitance C0 are determined using the following equations:

e-ISSN: 2582-5208
International Research Journal of Modernization in Engineering Technology and Science
(Peer-Reviewed, Open Access, Fully Refereed International Journal)
Volume:06/Issue:04/April-2024 Impact Factor- 7.868 www.irjmets.com

$$L_k = \frac{v_k \cdot D_k}{f_s \cdot \Delta I_k} \quad (1)$$

$$C_O = \frac{I_O \cdot (1 - D_k)}{f_s \cdot \Delta V_{CS}} \quad (2)$$

where k = 1 and 2, ΔV_{cs} is the voltage ripple of C_0, and:

$$\Delta I_k = C_k \frac{\Delta v_k}{D_k \cdot T_S} \quad (3)$$

2.2.1 ESS DISCHARGING DOMAIN

In a singular switching cycle, the switch can function in any of the four available modes. The waveforms of the recommended converter and the corresponding circuit are provided for reference.

Mode 1(a): During this mode, switches (S2) are turned on while switches (S3) are turned off. Diode (D1) is reverse biased.

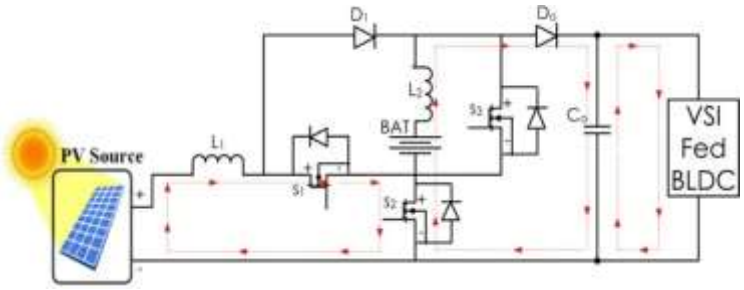

Figure 2.2: Discharging Domain Circuit Diagram ,Mode 1(a)

Figure 2.2 illustrates the equivalent circuit of the proposed converter. The input side inductor (L2) begins to charge from the PV source, causing the current (IL1) to rise. The inductor (L2) of the ESS and battery start discharging through the body diode (SD2) of switch (S2) to the output capacitor (C0). As a result, the current (IL2) decreases, and the output capacitor (C0) starts discharging to the load.

2.2.2 ESS CHARGING DOMAIN

During a single switching period, there exist four operational modes depending on the state of the switch. Mode 2 (a) entails the switches (S1) and (S2) being in the "ON" position, while diode D1 is reverse biased.

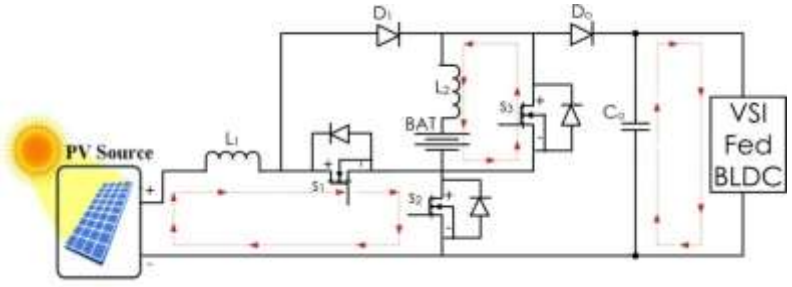

Figure 2.3: Charging Domain Circuit Diagram ,Mode 2(a).

The corresponding circuit of the proposed converter is shown in Figure 2.6. From the photovoltaic (PV) source, the inductor L1 on the input side begins to charge, and current iL1 increases. The inductor L2 on the ESS and the battery are beginning to charge through (SD3 body diode) of switch S3 to the output capacitor C0. Current iL2 is decreasing and output capacitor C0 begins to discharge to load.

2.3 MATHEMATICAL MODELING OF PROPOSED SYSTEM

2.3.1 PV MODELING

The mathematical representation of a PV module can be derived from the equivalent circuit of a PV solar cell. The photocurrent, denoted as Ic, is determined by the temperature and solar irradiation of the cell, while Rs and Rsh represent the series and shunt resistances of the PV cell. The nonlinear voltage-current characteristic of the PV solar cell can be assessed using the Equation.

$$I_{pv} = I_C - I_O \left[\exp\left(\frac{q(v_{Pv} + R_s I_{pv})}{kT} \right) - 1 \right] - \frac{v_{Pv} + R_s I_{pv}}{R_{sh}} \quad (4)$$

e-ISSN: 2582-5208
International Research Journal of Modernization in Engineering Technology and Science
(Peer-Reviewed, Open Access, Fully Refereed International Journal)
Volume:06/Issue:04/April-2024 Impact Factor- 7.868 www.irjmets.com

2.3.2 THE FLOW OF ELECTRICITY IN SOLAR CELL

Electrons, bearing a negative charge, migrate towards the front surface of the solar photovoltaic cell, resulting in an electrical charge imbalance. The electrical conductors on the cell then capture these electrons. Once the conductors are linked in an electrical circuit to an external load, like a battery, electricity is able to pass through the circuit.

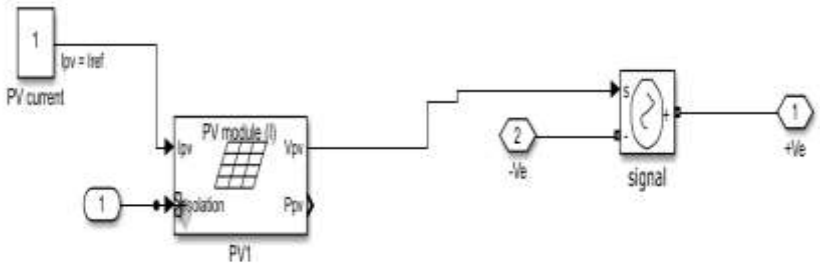

Figure 2.4: Simulation of PV

2.4 CONTROLLERS

This is the mechanism or algorithm responsible for processing the sensor input and producing the control output. It evaluates the measured process variable against the target set point and computes the error signal. Using this error signal, the controller produces the control output for the actuator.

2.4.1 VOLTAGE CONTROLLER

The DC-DC Voltage Controller block utilizes discrete-time proportional-integral (PI) DC-DC voltage control with feedforward (FF) for optimizing transient response. It can provide either a duty cycle or a current control signal. Additionally, an anti-windup gain is implemented to prevent integral gain saturation.

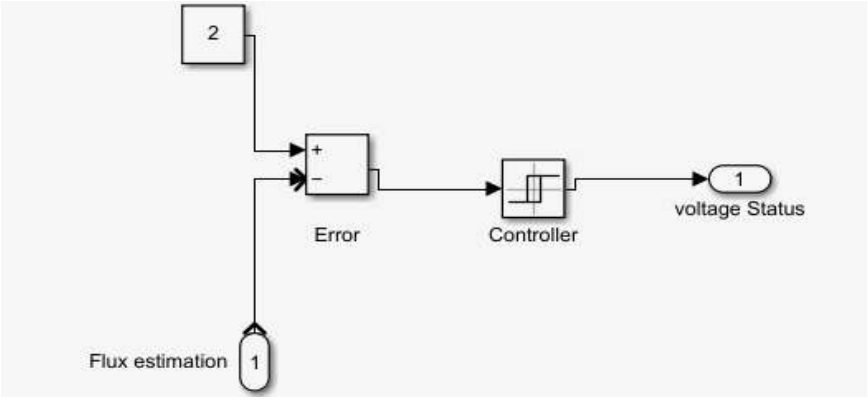

Figure 2.5: Simulation of Voltage Controller

Table 2: Controlled voltage source block properties

Source Type	DC
Initialize	On
Amplitude	230

2.4.2 PI CONTROLLER

The PI Proportional and Integral controller is a widely utilized technique in control systems to rectify the discrepancy between the desired setpoint and the actual value, based on feedback. Over the past decade, Permanent Magnet Brushless DC (BLDC) motors have found significant applications in various industries such as E-mobility (Electric vehicles, Electric bicycles), Industrial robots, and CNC machine tools. BLDC motors are crucial components in numerous industrial automation applications due to their exceptional efficiency and high torque-to-power ratios. Unlike traditional motors, Brushless DC motors operate without brushes on the rotor, resulting in minimal maintenance requirements. In the presented approach, the Hall Effect sensors are employed to commutate the BLDC motor. Furthermore, an algorithm is proposed for closed-loop PWM speed control of BLDC motors, where a predetermined value or user control is utilized to regulate the motor speed.

e-ISSN: 2582-5208
International Research Journal of Modernization in Engineering Technology and Science
(Peer-Reviewed, Open Access, Fully Refereed International Journal)
Volume:06/Issue:04/April-2024 Impact Factor- 7.868 www.irjmets.com

Table 3: Discrete PI Controller block properties

PARAMETER	SYMBOL	VALUE
Proportional gain	k_p	0.1
Integral gain	k_i	1
Sample time	-	50e-6
Output limits	Upper lower	1e6 10e6

2.4.3 PID CONTROLLER

Simultaneously, the PID controller's constant coefficients, namely Kp, Ki, and Kd, are utilized to establish a set of values. By incorporating these values, the modified controller suggested can be adapted to any desired dimension.

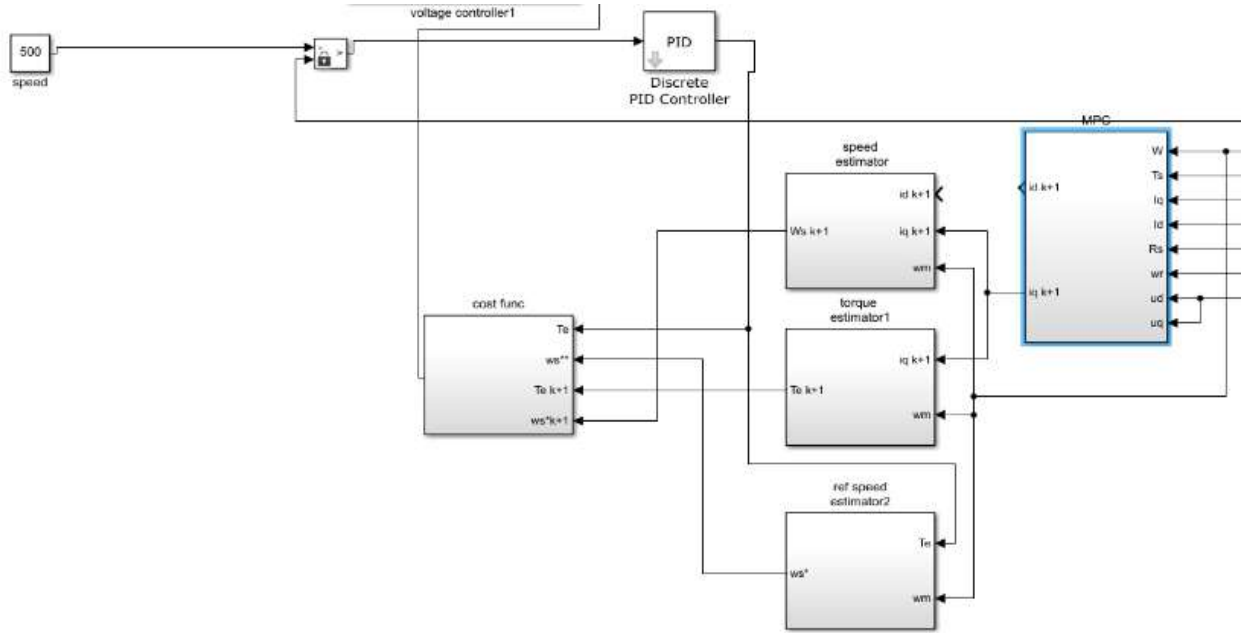

Figure 2.6: Simulation of PID Controller

Table 3: Discrete PID Controller Block Properties

Name	Kp	Ki	Kd	Tc D	Par Limits	Init	Ts
Discrete PID Controller	11.2	90	2.4	1	[100 -100]	0	0.5

III. SIMULATION PARAMETER SPECIFICATIONS

3.1 SIMULATION CIRCUIT

It has evolved over a period of years with input from many users. In university environments, it is the standard instructional toolfor introductory and advanced courses in mathematics, engineering, and science. In industry, MATLAB is the tool of choice for high-productivity research, development, and analysis. Its features a family of add-on application-specific solutions called toolboxes. Very important to most users of MATLAB, toolboxes allow you to learn and apply specialized technology. The figure displays the simulation circuit of the proposed system. The simulation was conducted using MATLAB 2021a version with the ode23tb solver. To execute the simulation and observe the outcomes, the discrete powergui with a time constant of 5e-7 was employed.

e-ISSN: 2582-5208
International Research Journal of Modernization in Engineering Technology and Science
(Peer-Reviewed, Open Access, Fully Refereed International Journal)
Volume:06/Issue:04/April-2024 Impact Factor- 7.868 www.irjmets.com

Table 4: Simulation parameter specification of Three port converter

PARAMETERS	SPECIFICATIONS
Inductor L_1	320 µH
Inductor L_2	320 µH
Capacitors C_0	1000 µF
Switch	3Power MOSFET
Diode	2PowerDiode
Switching frequency	50kHz
Input supply	1800 W
Cell Temperature	25^0 C
Irradiance	1000W/m^2

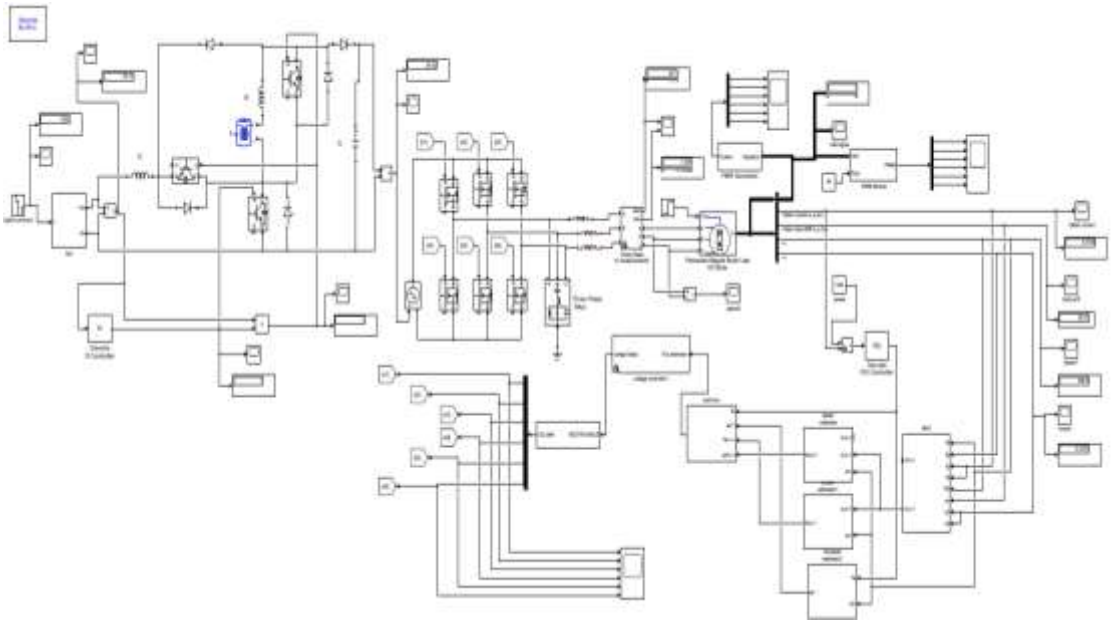

Figure 3.1 Simulation of TPC Circuit.

3.2 SIMULATION RESULT

The system simulation was created utilizing MATLAB/Simulink. A prototype of the DC-DC Converter under consideration has been constructed and examined. In order to attain the target output voltage, the simulation circuit was formulated in MATLAB, incorporating the necessary components available in MATLAB/Simulink.

3.2.1 PANEL VOLTAGE

The voltage obtained from the panel is depicted in Figure 3.1. The Simulink model utilizes a user-defined panel. By increasing the series and parallel strings, the desired voltage has been achieved.

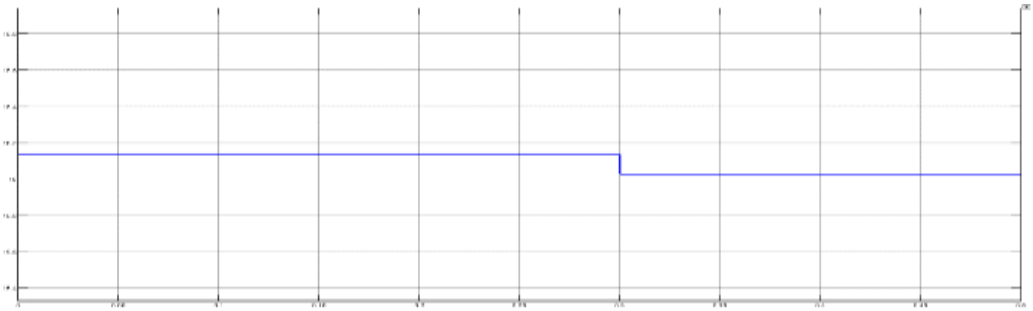

Figure 3.2: Waveform of PV

e-ISSN: 2582-5208
International Research Journal of Modernization in Engineering Technology and Science
(Peer-Reviewed, Open Access, Fully Refereed International Journal)
Volume:06/Issue:04/April-2024 Impact Factor- 7.868 www.irjmets.com

3.2.2 CONVERTER VOLTAGE

The output voltage obtained from the three port converter for the designed duty cycle is illustrated in Figure 3.2. By utilizing the three port converter, the voltage of the PV panel is effectively increased.

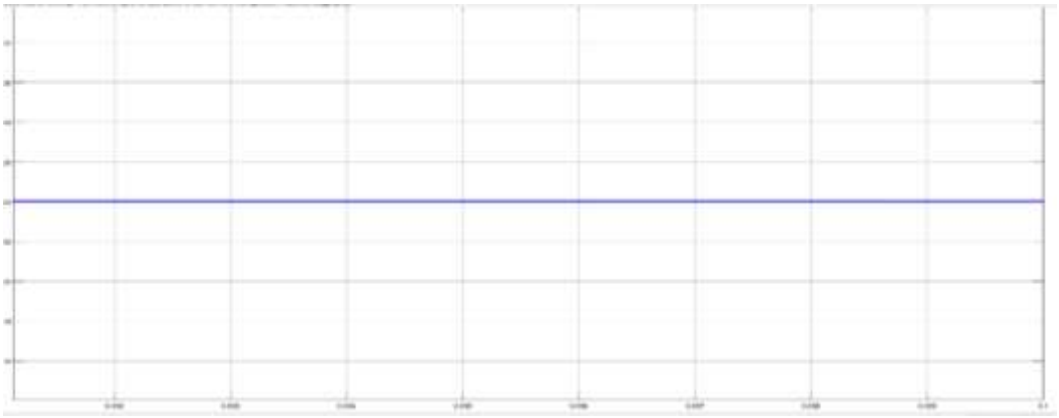

Figure 3.3: Waveform of Three Port Converter Voltage

3.2.3 UNIVERSAL BRIDGE

In Figures 3.3 and 3.4 depict the universal bridge with and without a filter. The plot was obtained prior to the filter being utilized in the circuit, showing ripples in the waveform.

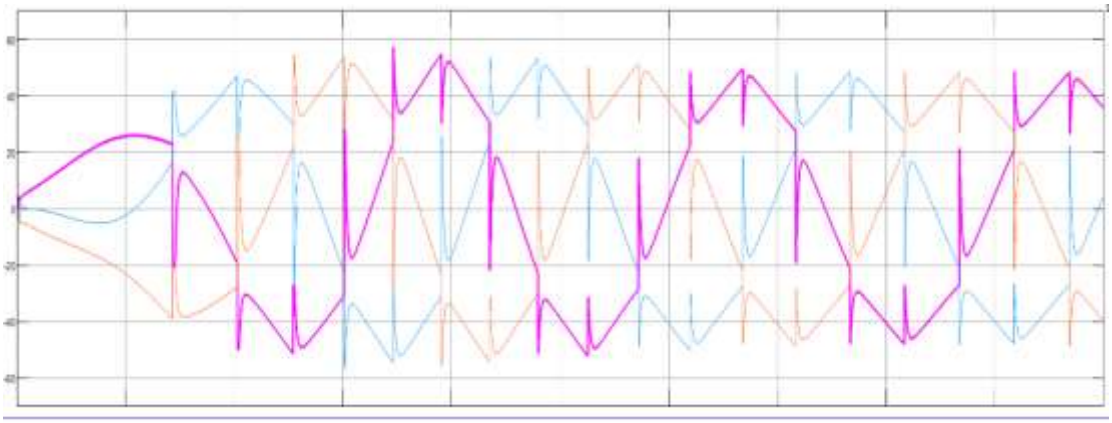

Figure 3.4 Waveform UB Without Filter

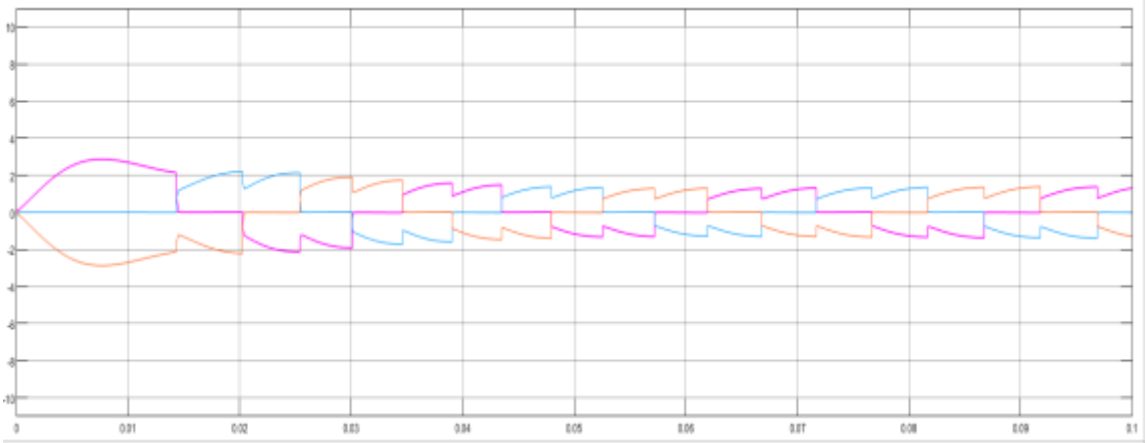

Figure 3.5: Waveform UB With Filter

3.2.4 SWITCHING PWM GENERATOR

The figure 3.6 shows the switching pulse width modulation given to the three port converter.

e-ISSN: 2582-5208
International Research Journal of Modernization in Engineering Technology and Science
(Peer-Reviewed, Open Access, Fully Refereed International Journal)
Volume:06/Issue:04/April-2024 Impact Factor- 7.868 www.irjmets.com

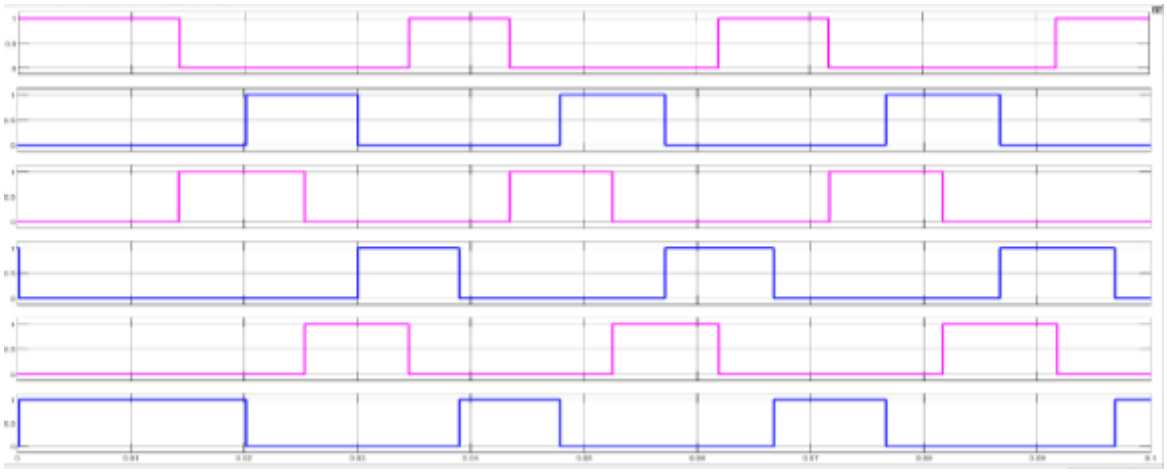

Figure 3.6: Waveform of Switching PWM Generator

3.2.3 BUS SELECTOR OF HALL SIGNAL

In this figure shown the hall signal that from bus selector of bldc.

Time (sec)

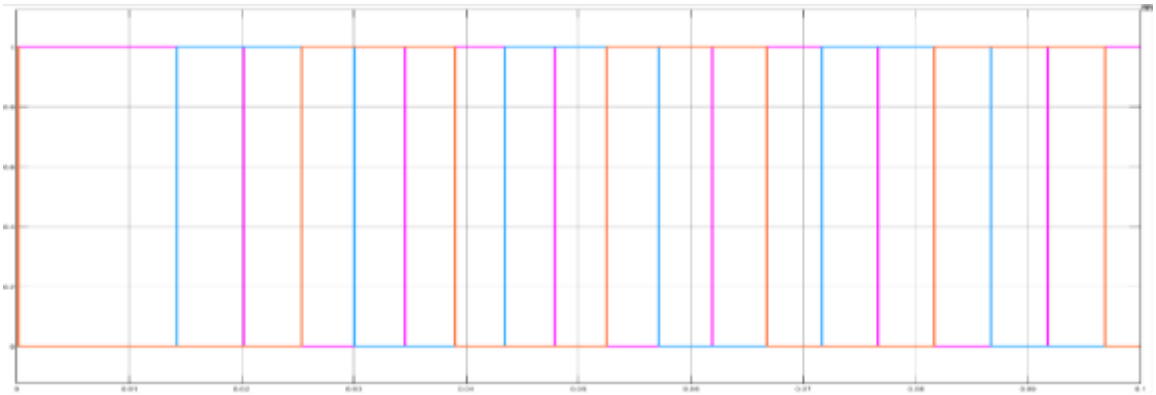

Figure 3.7: Waveform of Hall Signal

3.2.4 HALL SENSOR PWM MODULE

In figure 3.8 this shows using hall sensor for bldc motor with pulse with modulation for six phase.

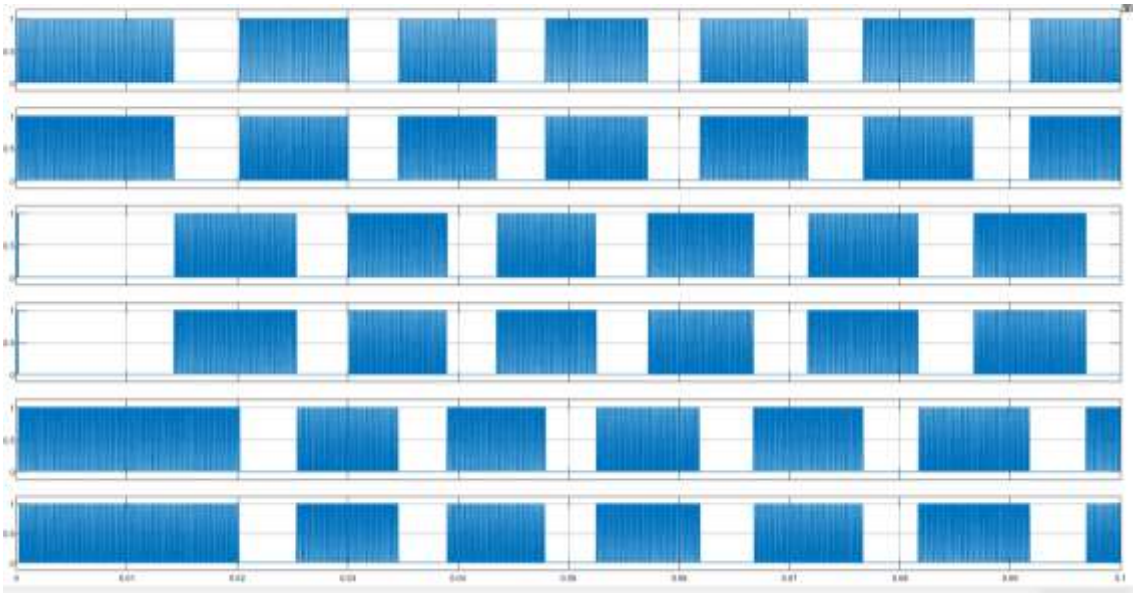

Time (sec)

Figure 3.8: Waveform Hall Sensor PWM Module

e-ISSN: 2582-5208
International Research Journal of Modernization in Engineering Technology and Science
(Peer-Reviewed, Open Access, Fully Refereed International Journal)
Volume:06/Issue:04/April-2024 Impact Factor- 7.868 www.irjmets.com

3.2.3 STATOR CURRENT

The simulation output waveform of the stator current is displayed in Figure 3.9. The time is represented on the X-axis, while the magnitude of current for the stator waveforms is shown on the Y-axis.

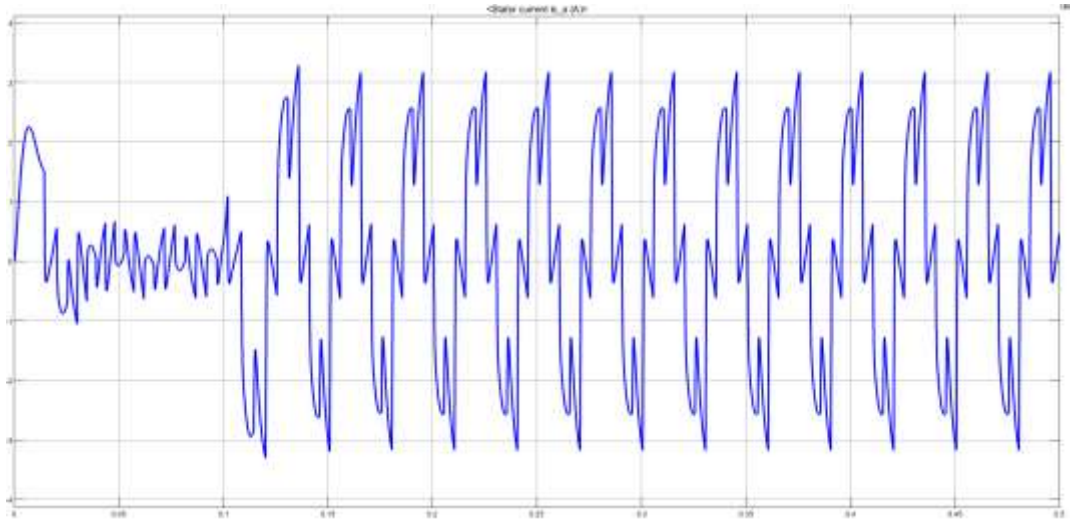

Time (sec)

Figure 3.9: Waveform of Stator Current

3.2.4 BACK EMF

In this figure 3.10 shows output waveform in the back emf X axis represent back emf and y axis represent angle.

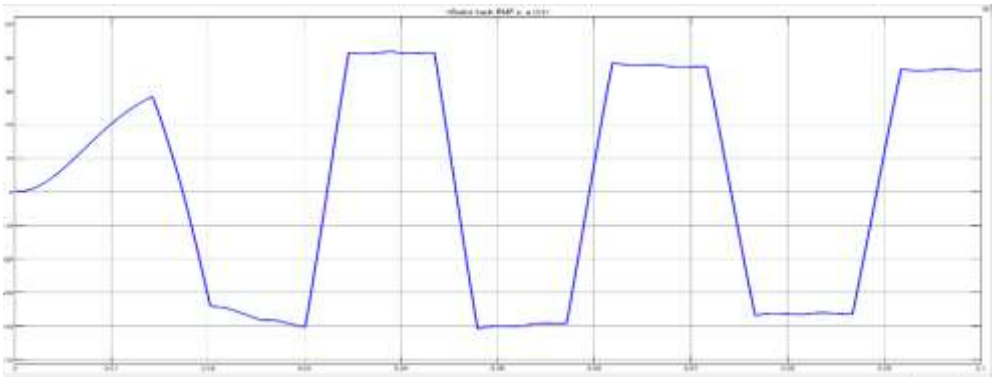

Time (sec)

Figure 3.10: Waveform of Back Emf

3.2.5 SPEED

In figure 3.11 shows output waveform of speed in BLDC motor ,to calculate speed by x axis is represents speed and y axis is represents time.

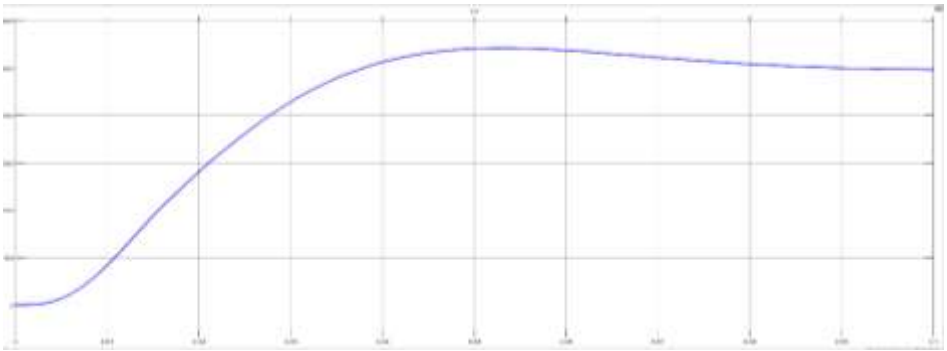

Time (sec)

Figure 3.11: Waveform of Speed

e-ISSN: 2582-5208
International Research Journal of Modernization in Engineering Technology and Science
(Peer-Reviewed, Open Access, Fully Refereed International Journal)
Volume:06/Issue:04/April-2024 Impact Factor- 7.868 www.irjmets.com

3.2.6 TORQUE

In figure 3.12 output waveform in torque from BLDC Shows, X axis represents Torque and Y axis represents time.

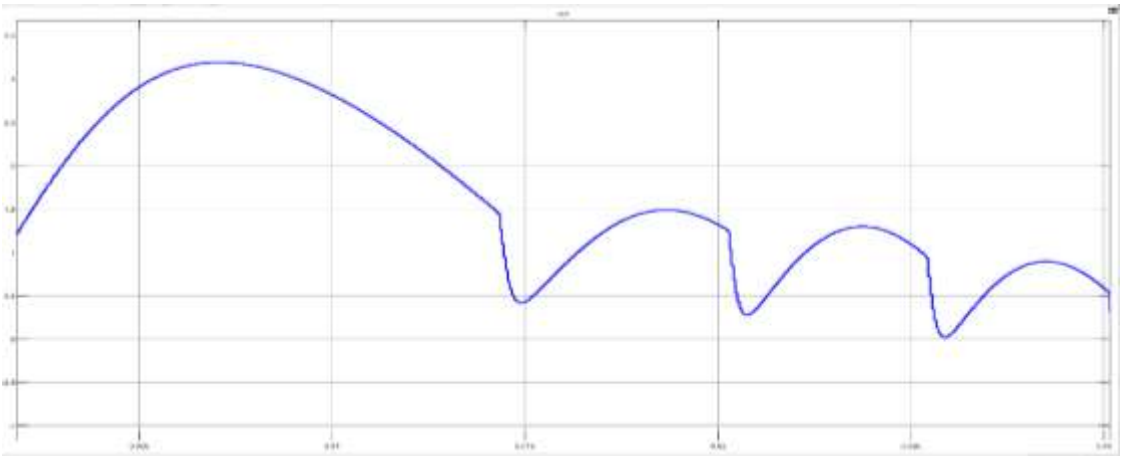

Time (sec)

Figure 3.12: Waveform of Torque

IV. CONCLUSION

In this study, we have introduced a novel three-port bidirectional DC-DC converter that combines solar PV and a battery to power a BLDC motor. This converter has been designed to efficiently manage power simultaneously. Unlike traditional converters, the power generation sources directly charge the battery, regardless of the load power. As a result, the overall output efficiency of the converter is significantly improved. The results clearly demonstrate that the converter is capable of maximizing power generation from solar PV during radiation and effectively controlling the battery to maintain a constant output value during irradiation. The proposed design exhibits an impressive efficiency of 96.5% while charging an ESS, 98.3% during discharge, and 95.76% when not charging an ESS. In the future, this innovative system can be implemented with a hysteresis comparator approach for automotive fuel pump applications.

V. REFERENCE

[1] Alijarajreh, H.; Lu, D.D.-C.; Siwakoti, Y.P.; Tse, C.K.A Nonisolated Three-Port DC–DC Converter with Two Bidirectional Ports and Fewer Components. IEEE Trans. Power Electron. 2022, 37, 8207–8216.

[2] Al-Atrash, H.; Tian, F.; Batarseh, I. Tri-modal half-bridge converter topology for three-port interface. IEEE Trans. Power Electron.**2021**, 22, 341–345.

[3] Hu, H.; Harb, S.; Fang, X.; Zhang, D.; Zhang, Q.; Shen, Z.J.; Batarseh, I. A three-port flyback for PV microinverter applications with power pulsation decoupling capability. IEEE Trans. Power Electron. **2012**, 27, 3953–3964.

[4] Krishnaswami, H.; Mohan, N. Three-port series-resonant dc–dc converter to interface renewable energy sources with bidirectional load and energy storage ports. IEEE Trans. Power Electron. **2019**, 24, 2289–2297.

[5] Wang, Z.; Li, H. An integrated three-port bidirectional DC–DC converter for PV application on a DC distribution system. IEEE Trans. Power Electron. **2022**, 28, 4612–4624.

[6] Wang, P.; Wang, W.; Xu, D.; Lu, X. A hardware decoupling method for series-resonance-based isolated three-port DC/DC converters. In Proceedings of the IEEE Applied Power Electronics Conference and Exposition (APEC), SanAntonio, TX, USA, 4–8 March 2018

[7] Wang, L.; Wang, Z.; Li, H. Asymmetrical duty cycle control and decoupled power flow design of a three-port bidirectional DC-DC converter for fuel cell vehicle application. IEEE Trans. Power Electron. **2011**, 27, 891–904.

[8] Wu, H.; Chen, R.; Zhang, J.; Xing, Y.; Hu, H.; Ge, H. A family of three-port half-bridge converters for a stand-alone renewable power system. IEEE Trans. Power Electron.

[9] Zhang, B.; Hong, D.; Wang, T.; Zhang, Z.; Wang, D. A novel two-phase interleaved parallel bi-directional DC/DC converter.Arch. Electr. Eng. **2021**,70,219–231.

[10] Wu, Y.-E. Novel High-Step-Up/Step-Down Three-Port Bidirectional DC/DC Converter for Photovoltaic Systems. Energies 2022,15, 5257.

[11] Marei, M.I.; Alajmi, B.N.; Abdelsalam, I.; Ahmed, N.A. An integrated topology of three-port dc-dc converter for PV-battery power systems. IEEE Open J. Ind. Electron. Soc. 2022, 3, 409–419.

[12] Kumar, M.; Barbosa, P.M.; Ruiz, J.M.; Minli, J.; Hao, S. Isolated Three-Port Bidirectional DC-DC Converter for Electric Vehicle Applications. In Proceedings of the IEEE Applied Power Electronics Conferenceand Exposition (APEC), Houston, TX, USA, 20–24 March 2022.

[13] Zahra Saadatizadeh;H.Alan Mantooth.;Expandable isolated bidirectional three-port DC-DC converter with high voltage conversion ratio for PV-Battery systems.IEEE Transportation Electrification Conference & Expo(ITEC)2023.

[14] Andressa Barbieri Moro; Wesley Biffe; António Manuel Santos Spencer Andrade, Three-Port DC-DC Converter Based on Ladder Switched Capacitor 2023 IEEE 8th Southern Power Electronics Conference and 17th Brazilian Power Electronics Conference (SPEC/COBEP)

[15] Anmol Ratna Saxena; Ashima Kulshreshtha A Three-Port DC-DC Converter for Solar PV Integration in DC Off-Grid Systems: Design and Control IEEE International Conference on Energy Technologies for Future Grids (ETFG). 2023

[16] Xiangxiang Zhang;Zhenpeng Luo;Huihui Wang;Siqing Zhang;Xiangyue Han;Ran Li Control strategy study of photovoltaic power supply for boost-type three-port converter,2023 IEEE International Conference on Sensors, Electronics and Computer Engineering (ICSECE)

[17] Wesley Biffe;Andressa Barbieri Moro;António Manuel Santos Spencer Andrade 2023 Non-pulsating Input and Output Transformerless Three-Port DC-DC Converter, 15th Seminar on Power Electronics and Control (SEPOC).

[18] Zahra Saadatizadeh;H. Alan Mantooth,Three-Port High Voltage Conversion Ratio DC-DC Converter 2022 IEEE 7th Southern Power Electronics Conference (SPEC).

[19] Lan Ma;Rui Fu;Xiaoqi Cao;Zeliang Shu,Isolated Three-Port Bidirectional Resonant Converter with Notch Filters,IECON 2023- 49th Annual Conference of the IEEE Industrial Electronics Society.

[20] Modal Analysis of Photovoltaic Power Supply Circuit for Boost-Type Three Port Converter,Xiangxiang Zhang;Zhenpeng Luo;Siqing Zhang;Baofeng Yang;Huihui Wang,2023 IEEE International Conference on Image Processing and Computer Applications (ICIPCA).

[21] Wu, Y.-E. Novel High-Step-Up/Step-Down Three-Port Bidirectional DC/DC Converter for Photovoltaic Systems. Energies 2022,15, 5257.